Online Measurements of the Fast Changing Dielectric Constant in Oil Shale Due to High-Power Microwave Heating

CHIA-LUN J. HU

Abstract—**The change of the complex dielectric constant $\bar{\epsilon}$ of oil shale under intensive microwave heating is an abrupt phenomenon which is quite different from that due to conventional heating. Based on the principle of competitive chemical kinetics, a theory is proposed here for explaining this rapid change of the dielectric constant. A mathematical analysis of a coaxial waveguide loaded with oil-shale blocks which has a fast changing $\bar{\epsilon}$ with respect to time is carried out in detail, from which an online measuring technique is derived for measuring this fast changing $\bar{\epsilon}$ with respect to time and temperature. Preliminary experimental results show that the proposed theory is suitable for explaining this fast changing phenomenon. The online measuring technique reported here is very similar to the three-probe or five-port measuring methods reported in the literature, except that it is more general compared to some of these methods. Its designing approach is also different because it is derived from a modified phasor analysis with the physical picture easily visualized.**

I. Physical Picture of a Dielectric Constant Changing Under Fast Microwave Heating

IT IS WELL KNOWN that microwave heating applied to many chemical substances will result in different products and different changes in physical–chemical properties as compared to those due to conventional heating. One main reason for this difference is that microwave heating is a fast heating process while conventional heating is a slow heating process. Suppose that when the temperature increases, a substance A is decomposed through the following two-path chemical reactions (which may include a change of phases):

$$A \xrightarrow{k_1} B + C \quad (1)$$

$$A \xrightarrow{k_2} D + E \quad (2)$$

and reaction constants k_1 and k_2 expressed by the "modified" Arrhenius relation (see, for example, [1]) (A and B in these equations are determined by the difference of energy levels between reactants and products, and by the statistical distribution of molecules among different levels (see, for example, [2])):

$$k_1 = A_1 T e^{-B_1/T} \quad (3)$$

Manuscript received September 15, 1977; revised January 31, 1978. This work was supported in part by the National Science Foundation.

The author is with the Department of Electrical Engineering, University of Colorado, Boulder, CO 80309.

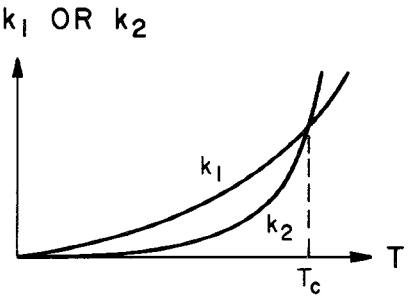

Fig. 1. Competitive chemical reaction rates.

$$k_2 = A_2 T e^{-B_2/T} \quad (4)$$

are sketched as shown in Fig. 1. Then we see that if the temperature T increases slowly, k_1 is much larger than k_2 during most of the time this slow heating process is taking place. Therefore, reaction (1) will predominate, and the thermally decomposed products will be mostly B and C. On the other hand, if T is brought beyond T_c (the cross-over temperature as shown in Fig. 1) in a very short time, then the second reaction will prevail, and the products will be mostly D and E. Since, in general, the average physical properties of D and E are different from those of B and C, a significant difference in the dielectric constant (among other things) may exist between products due to fast heating and those due to slow heating.

Our preliminary experiment[1] shows that the change of the complex dielectric constant of virgin oil shale under microwave heating is quite abrupt around 465°C, but with conventional heating no such abrupt change was observed. These two results are schematically sketched in Fig. 2. The sharp change in $\bar{\epsilon}$ under the fast heating process can be directly explained from the characteristic of the $(k_2 - T)$ curve in Fig. 1 when the temperature is brought beyond T_c in a short time. The above theory of

[1]We heat a rectangular oil-shale sample in a microwave oven with a thermometer attached to the shale. When the temperature rises to a certain level, we take the sample out and use a standard waveguide-traveling-probe method to measure its input impedance and therefore its $\bar{\epsilon}$. Repeating this with different samples at different temperatures, we observe qualitatively, if not quantitatively, that an abrupt decrease of $\bar{\epsilon}$ occurs around 465°C. We also ran similar experiments using conventional heating (induction heating). The results of these two sets of experiments are roughly sketched as shown in Fig. 2.

0018-9480/79/0100-0038$00.75 ©1979 IEEE

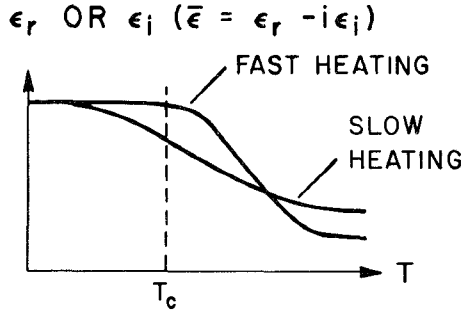

Fig. 2. Temperature dependence of oil-shale dielectric constants under different heating processes.

the $(\bar{\epsilon}-T)$ relation under microwave heating depends, of course, on the existence of a set of competitive reaction paths with significant differences among kinetic constants. It is well known in petroleum chemistry that during the thermal cracking of crude oil, the products will depend critically on the temperatures [3], [4] and the time taken to reach these temperatures [3]–[6]. Oil shale is a complex organic medium having major constituents comparable to those of crude oil. Consequently, the theory proposed here for explaining fast-change oil-shale properties under microwave heating is a reasonable one.

In Section II, a system consisting of a coaxial waveguide loaded with oil-shale blocks under microwave heating is analyzed. From this analysis, an online measuring technique is derived which allows the fast changing $\bar{\epsilon}$ to be measured instantaneously while the shale is heated by microwave energy.

II. Analysis of an Oil-Shale-Loaded Parametric Waveguide

To simplify the calculation, let us assume that the $(\bar{\epsilon}-T)$ curves (Fig. 2) of the oil shale under a fast heating process can be approximated by two broken lines as shown in Fig. 3, where ϵ_r and ϵ_i are the real and imaginary parts of the complex dielectric constants $\bar{\epsilon}$ (i.e., $\bar{\epsilon}\equiv\epsilon_r - i\epsilon_i$) at a fixed frequency 915 MHz—the frequency of the 1-kW microwave generator we are now using. ϵ_{r0} and ϵ_{i0} are the initial values before the heating process is applied, T_c is the "critical" temperature (see Fig. 1) where abrupt changes start, and T_d is the "ending-point" temperature where all chemical reactions in the heated region reach completion. Under this idealization of the $(\bar{\epsilon}-T)$ curves, the following analysis says that measuring $\bar{Z}_{in}$ of the oil-shale-loaded coaxial guide *online* (meaning measuring $\bar{Z}_{in}$ at each instant while the oil shale is heated by microwave), we can calculate the slopes α and β of the fast changing sections of the curves shown in Fig. 3. If the slopes thus calculated are about the same for each $\bar{Z}_{in}$ we measure online, the whole theory is then checked experimentally.

The fast-changing central sections of the $(\bar{\epsilon}-T)$ curves in Fig. 3 can be expressed analytically by

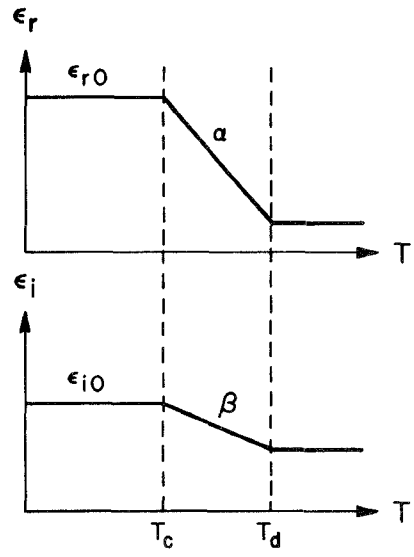

Fig. 3. Idealized $(\bar{\epsilon}-T)$ curves of oil shale under fast heating process.

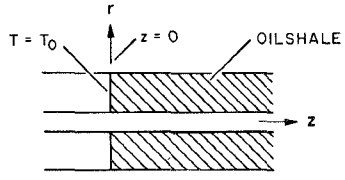

Fig. 4. Oil-shale-loaded coaxial waveguide.

$$\left.\begin{aligned}\epsilon_r &= \epsilon_{r0}-\alpha(T-T_c)\\ \epsilon_i &= \epsilon_{i0}-\beta(T-T_c)\end{aligned}\right\}, \quad \text{when } T_d \geqslant T \geqslant T_c$$

or

$$\bar{\epsilon}=\bar{\epsilon}_0\left[1-\bar{X}(T-T_c)\right], \qquad \text{when } T_d \geqslant T \geqslant T_c \tag{5}$$

where $\bar{\epsilon}\equiv\epsilon_r - i\epsilon_i$, $\bar{\epsilon}_0\equiv\epsilon_{r0}-i\epsilon_{i0}$, and $\bar{X}\equiv(\alpha-i\beta)\bar{\epsilon}_0^{-1}$, while, when $T<T_c$, we have

$$\bar{\epsilon}=\bar{\epsilon}_0=\text{constant}. \tag{6}$$

Combining (5) and (6) gives us an analytical expression for $\overline{\Delta\epsilon}$:

$$\frac{\overline{\Delta\epsilon}}{\bar{\epsilon}_0}\equiv\frac{\bar{\epsilon}_0-\bar{\epsilon}}{\bar{\epsilon}_0}\equiv-\bar{X}S(T-T_c), \qquad \text{when } T<T_d \tag{7}$$

where S represents a unit step function.

Now, if we fill a coaxial waveguide with toroidal-shaped sections of oil shale (Fig. 4) and design the diameters of the inner and outer conductors in such a way that only the TEM mode can pass through the guide with E and H fields almost constant at each point in the cross section, then, when we send the microwave power into the waveguide, the power P propagating down the guide will attenuate along the z axis according to $e^{-2k_{0i}z}$ where $k_{0i}\equiv -\text{Im}\,\omega\sqrt{\mu_0\bar{\epsilon}_0}$. We use $e^{+i\omega t}$ as the time factor in the analysis; thus the propagation factor of the TEM mode is $e^{-i\bar{k}_0 z}$ where $\bar{k}_0\equiv k_{0r}-ik_{0i}\equiv\omega\sqrt{\mu_0\bar{\epsilon}_0}$. Therefore, the attenuation factor is $|e^{-i\bar{k}_0 z}|\equiv e^{-k_{0i}z}$ where $k_{0i}\equiv -\text{Im}\,\bar{k}_0$.

Because of the fact that the power attenuated is turned into heat, the temperature rise in the oil shale (which is

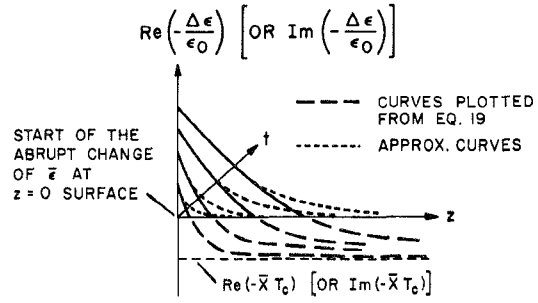

Fig. 5. Propagation of dielectric perturbation during the fast heating process.

proportional to $-\partial P/\partial z$) is

$$\Delta T = T_0 e^{-2k_{0i}z} \tag{8}$$

where T_0 is the temperature rise (i.e., the increment temperature beyond the ambient temperature) at the entrance surface (where $z=0$) of the oil shale. The conduction of heat during this fast heating process is neglected. T_0 here will be an increasing function of time during the heating process. From Fig. 3 we see that $\bar{\epsilon}$ is a constant until T_0 reaches the critical temperature T_c at which an abrupt change of $\bar{\epsilon}$ commences. After the T_c point is reached, the waveguide becomes a parametric waveguide because $\bar{\epsilon}$ is no longer a constant along the guide. The normalized change of $\bar{\epsilon}$ along z, according to (7) and (8), will be

$$\frac{\overline{\Delta\epsilon}}{\bar{\epsilon}_0} = -\bar{X}S\left(T_0 e^{-2k_{0i}z} - T_c\right). \tag{9}$$

A plot of this $\overline{\Delta\epsilon}$ versus z when time t increases is schematically shown in Fig. 5. These ($\overline{\Delta\epsilon}-z$) curves are broken exponential curves as shown by the solid lines in the figure. The interception on the vertical axis is equal to Re $[\bar{X}(T_0-T_c)]$ or Im $[\bar{X}(T_0-T_c)]$ which increases with time t because T_0 increases with t.

Now since these broken exponential curves are not too convenient to handle analytically (in reality, they are not broken curves, and the broken parts are due to the idealization of the ($\bar{\epsilon}-T$) curves shown in Fig. 3), we will approximate them by a set of pure exponential curves such that $\overline{\Delta\epsilon}$ and $d\overline{\Delta\epsilon}/dz$ at $z=0$ are kept unchanged. The analytical expression for these approximated curves (shown by the short dots in Fig. 5) can be calculated from (9), becoming

$$\frac{\overline{\Delta\epsilon}}{\epsilon_0} = -\bar{X}(T_0-T_c)e^{(-2k_{i0}T_0/T_0-T_c)z}, \qquad \text{when } T_0 \geqslant T_c$$

$$\equiv -\bar{A}e^{-2bz} \tag{10}$$

where

$$\bar{A} \equiv \bar{X}(T_0-T_c) \text{ is a complex number} \tag{11a}$$

and

$$b \equiv \frac{k_{i0}T_0}{T_0-T_c} \text{ is a positive real number.} \tag{11b}$$

With (10) in mind, we can then solve the wave equation for this parametric waveguide. From this, we can obtain an exact expression of $\bar{Z}_{in}$ as a function of T_0 and the unknown temperature coefficient $\bar{X}$. Measuring $\bar{Z}_{in}$ and T_0 online, we can finally calculate $\bar{X}$ or α and β, the slopes of the ($\bar{\epsilon}-T$) curves shown in Fig. 3. Other assumptions used in the analysis are that the E and H fields are almost constant over any cross section of the coaxial waveguide because only the TEM mode is excited, and these E and H fields only see the isotropic part of the anisotropic ϵ and μ tensors of the oil shale because the shale is cut with the cylindrical axis perpendicular to the layered surface.

A. Waveguide Analysis

Under the above assumptions, we can separate the wave equation by the standard technique of separation of variables and obtain the following equation:

$$\frac{d^2E}{dz^2} + \left[\bar{k}_0^2 - \bar{k}_1^2 e^{-2bz}\right]E = 0 \tag{12}$$

where E is the E field along the radial direction of the coaxial guide $\bar{k}_0^2 \equiv \omega^2\mu_0\bar{\epsilon}_0$. $\bar{\epsilon}_0$ is the unperturbed oil-shale dielectric constant. $\bar{k}_0$ is a complex number because $\bar{\epsilon}_0$ is. $\bar{k}_1^2 \equiv \bar{A}\bar{k}_0^2$ where $\bar{A}$ is given by (11). That is, in (12),

$$\bar{k}_0^2 \equiv \omega^2\mu_0\bar{\epsilon}_0 \qquad \text{is a complex constant}$$

$$\bar{k}_1^2 \equiv \omega^2\mu_0\bar{\epsilon}_0\bar{X}(T_0-T_c) \qquad \text{is an unknown complex constant}$$

$$b \equiv \frac{k_{i0}T_0}{T_0-T_c}, \qquad \text{where } k_{i0} \equiv -\operatorname{Im}\bar{k}_0. \tag{13}$$

In (13) $\bar{X}$ and T_0 (entrance temperature of the oil shale) are the only unknowns to be measured by the online technique discussed in the next section.

Using a transformation of variable given by $U = \bar{k}_1 e^{-bz}$ with

$$\frac{d}{dz} = \frac{dU}{dz}\frac{d}{dU} = -bU\frac{d}{dU}$$

and

$$\frac{d^2}{dz^2} = \frac{dU}{dz}\frac{d}{dU}\left(-bU\frac{d}{dU}\right) = b^2U\frac{d}{dU} + b^2U^2\frac{d^2}{dU^2}$$

one can convert (12) to

$$\frac{d^2E}{dU^2} + \frac{1}{U}\frac{dE}{dU} + \left(\frac{k_0^2}{b^2U^2} - \frac{1}{b^2}\right)E = 0.$$

Comparing this with the standard Bessel equation, we see immediately that the solutions of this equation are the modified Bessel functions of complex orders and complex arguments. That is

$$E = E_0 I_{(i\bar{k}_0/b)}\left(\frac{\bar{k}_1}{b}e^{-bz}\right) \text{ or } E_0 K_{(i\bar{k}_0/b)}\left(\frac{\bar{k}_1}{b}e^{-bz}\right)$$

where E_0 is a constant determined by the incident field strength at the $z=0$ plane. The choice between these two solutions I and K is determined by the boundary condi-

tion that, as $z\to\infty$, E should approach $e^{-i\bar{k}_0 z}$. (This is equivalent to saying that when z approaches infinity, the perturbation on $\bar{\epsilon}$ is zero; therefore, we expect the wave there to be a regular forward propagating wave.) When $z\to\infty$, $(\bar{k}_1/b)e^{-bz}\to 0$. Therefore, using the series expansion of $I_\nu(\eta)$ near $\eta=0$ point, or [7]

$$I_\nu(\eta)=\frac{\left(\frac{1}{2}\eta\right)^\nu}{\Gamma(\nu+1)}\left\{1+\frac{\left(\frac{1}{2}\eta\right)^2}{\nu+1}+\frac{\left(\frac{1}{2}\eta\right)^4}{2!(\nu+1)(\nu+2)}+\cdots\right\}$$

we see that

$$I_{(i\bar{k}_0/b)}\left(\frac{\bar{k}_1}{b}e^{-bz}\right)\cong B\left(\frac{\bar{k}_1}{b}e^{-bz}\right)^{(i\bar{k}_0/b)}$$
$$=B'e^{-i\bar{k}_0 z}$$

where B and B' are two irrelevant complex constants.

On the other hand, expanding $K_\nu(\eta)$ near zero will not give us a convergent result. Therefore, I must be the only correct solution. Finally, from the equations that $\bar{Z}_{in}\equiv E_r/H_\theta$ and $H_\theta\equiv(i/\omega\mu_0)(\partial E_r/\partial z)$, we have (using formula $I'_\nu(\eta)=(\nu/\eta)I_\nu(\eta)+I_{\nu+1}(\eta)$) [7],

$$(\bar{Z}_{in})_{z=0}=i\omega\mu_0\frac{I_{(i\bar{k}_0/b)}\left(\frac{\bar{k}_1}{b}\right)}{\bar{k}_1\left[i\frac{\bar{k}_0}{\bar{k}_1}I_{(i\bar{k}_0/b)}\left(\frac{\bar{k}_1}{b}\right)+I_{(i\bar{k}_0/b)+1}\left(\frac{k_1}{b}\right)\right]} \tag{14}$$

where $\bar{k}_0$, $\bar{k}_1$, and b are given by (13) with $\bar{X}$ and T_0 being the only unknown constants.

III. Experiments

A. Principle of Online Impedance Measurements

The online measuring method used here is very similar to the multiple-probe methods [8]–[10] and five- or six-port techniques [11], [12] reported in the literature, but it is derived from a different point of view as shown in the following.

Suppose we sample at three arbitrary points on a lossless waveguide terminated by the unknown impedance $\bar{Z}_{in}$ as shown in Fig. 6; then, from the sampled fields $|\bar{E}_1|$, $|\bar{E}_2|$, and $|\bar{E}_3|$ we can determine not only the magnitude but also the phase of the unknown impedance $\bar{Z}_{in}$. The following is a modified transmission-line phasor analysis which will lead us to the determination of $\bar{Z}_{in}$ by means of a geometrical technique used in conjunction with a conventional Smith chart.

Let the horizontal unit vector $\overline{L0}$ in Fig. 7 represent the forward E wave (electric field wave) at the loading point L of Fig. 6 and vector $\overline{0R}$ represent the reflected E wave at that point. Then the resultant E field at the loading point will be represented by vector LR ($\overline{LR}\equiv\overline{L0}+\overline{0R}$). If the reflected wave $\overline{0R}$ is taken as the reference vector (in contrast to the conventional phasor analysis in which the forward wave is usually taken as the reference vector), then when we move towards the generator by a distance l_3 to sampling point 3 (Fig. 6), the phase of the forward wave will be advanced[2] by βl_3 while that of the reflected wave will be retarded by βl_3 where β is the propagation constant in the lossless guide. Therefore, the phasor relation between these two waves at point 3 will be represented by $\overline{30}$ (forward wave) and $\overline{0R}$ (reflected wave) with angle $30L$ equal to $2\beta l_3$ as shown in Fig. 7. Hence the sampled magnitude at point 3 is proportional to the magnitude of vector $\overline{3R}$ which is the resultant vector of $\overline{30}+\overline{0R}$. Similarly, the sampled magnitude at point 2 will be proportional to the magnitude of $\overline{2R}$ and that at point 1 to the magnitude of $\overline{1R}$ as shown in Fig. 7. Since the relative positions of points 1, 2, 3, and L on the circumference of the diagram in Fig. 7 can be determined easily if we know l_1, l_2, l_3, and β, and the ratio $1R:2R:3R$ ($\equiv$ ratio of the resultant E fields at points 1, 2, $3\equiv|\bar{E}_1|:|\bar{E}_2|:|\bar{E}_3|$) can be measured by the three samplers, the position of point R in the diagram can be determined exactly. Then the relative magnitude and phase of the reflected E wave $\overline{0R}$ are measurable on the diagram with respect to the forward wave $\overline{L0}$. Since $\overline{L0}$ is a horizontal unit vector, $\overline{0R}$ will be equal to the loading point reflection coefficient $\bar{k}$ because $\bar{k}\equiv\overline{0R}/\overline{L0}=\overline{0R}$. Consequently, the normalized impedance $\bar{z}_{in}$ at the loading point can be determined immediately by superimposing Fig. 7 over a conventional Smith chart with the center 0 and the leftmost point L coinciding to the center and the leftmost point of the Smith chart, respectively.

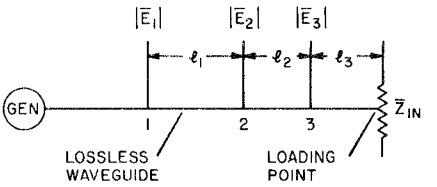

Fig. 6. A three-point sampling system for measuring $\bar{Z}_{in}$ online.

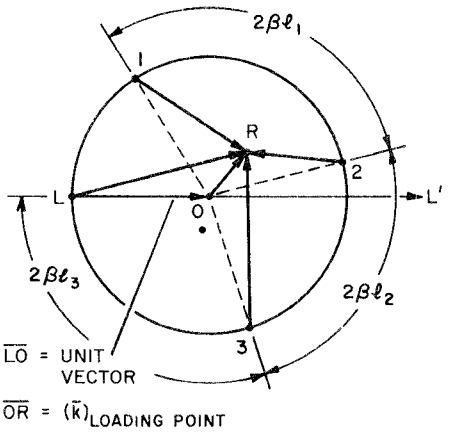

Fig. 7. Phasor diagram of the three-point sampling system.

[2]For example, forward wave at point 3 reaches the same phase earlier than that at point L does.

To determine the position of point R in Fig. 7 by means of the sampling ratio $1R:2R:3R$ and the relative locations of probes 1, 2, and 3 with respect to the loading point L, we can use the following principle.

From elementary geometry, if the base AB of a triangle ABC and the ratio $r \equiv AC:BC$ are fixed, the trajectory of the vertex C is a circle. The center and the radius of this circle can be determined uniquely by $\overline{AB}$ and r. Based on this theory, we can construct two circular trajectories of point R. The first trajectory is based on line $\overline{12}$ in Fig. 7 and the measured ratio of $r_{12} \equiv |\bar{E}_1|/|\bar{E}_2|$ which is equal to $1R:2R$. The second trajectory is based on line $\overline{23}$ (or line $\overline{13}$) and the measured ratio of $2R:3R$ (or $1R:3R$). The intersecting point of these two trajectories is point R from which we can determine $\bar{z}_{in}$ by means of a Smith chart as just described. In fact, we can construct two sets of circular contours on a conventional Smith chart based on this trajectory analysis. Each contour will correspond to a particular value of $|\bar{E}_1|/\bar{E}_2|$ or $|\bar{E}_2|/|\bar{E}_3|$ from which we can determine $\bar{z}_{in}$. (A detailed analysis on this and the generalized measuring technique will be discussed in a forthcoming paper.)

B. Experimental Setup and Measurements

The experimental arrangement of Fig. 8 was used for measuring T_0 and $\bar{Z}_{in}$ online while oil shale is being heated by 700–900 W of microwave power.

To measure the fast changing T_0 online, we use a chromel–alumel or type-K thermocouple attached to the entrance surface and let the two wires coming out of the end plate through the central conductor of the coaxial guide as shown in Fig. 8. The reference temperature is at the input of the difference amplifier which is 3 ft away from the coaxial waveguide and, hence, at room temperature (25°C). The difference amplifier has a balanced double-ended input and a single-ended grounded output. The dc offset circuit is used to offset the large dc temperature before reaching the critical temperature T_c such that a small but fast temperature change beyond T_c can be displayed and recorded clearly on the storage oscilloscope.

The microwave generator generates a maximum CW microwave power of 1000 W at 915 MHz. The output of this generator is connected to a 1+5/8-in standard air-dielectric coaxial guide. The double-stub tuner is designed with compatible dimensions to the main coaxial guide. It is used to match the impedance seen by the generator such that the reflected power sent into the generator is minimized. The cross-hatched section in Fig. 8 is the oil-shale-loaded section. It is 6 ft long and cut into toroidal sections fitting to the coaxial guide. The orientation of the cutting is such that the toroidal axis is perpendicular to the layered surfaces of the oil shale. The gas exhaustion tube is a 1/4-in brass tube 2 ft long. The small diameter and the length of the tube assure that it is below cutoff at the measurement frequency. The detectors used in the samplers are conventional 1N23C-type square-law

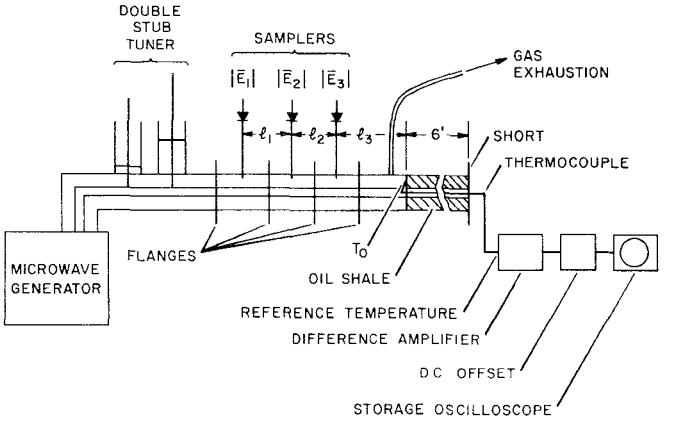

Fig. 8. Experimental setup.

TABLE I

$V_{thermocouple}$ (mV)	0	18.3	20.1	21.6
T_0 (ref=25°C) (°C)	25	469	511.5	548
Sampled outputs (Relative values) D_1		9	11.8	12.1
D_2		5.24	6.87	12.1
D_3		7.9	13.9	22.8
$\bar{r}$ (calculated by eqs. 5 and 15 and the data recorded here)	4-j0.32	3.89-j0.276	3.64-j0.18	3.34-j0.09

detectors. The outputs of the detectors are connected to three oscilloscopes. The samplers are calibrated by the following method. First, we put a short to the end of the sampling section and turn the generator on to a low-level output (10–30 W). Then we adjust the probing depths of the samplers such that when we change the order of the positions of the samplers, the monitored output at a fixed position is always the same no matter which sampler is connected there. With these samplers adjusted, we then connect the oil-shale-loaded section on, turn the generator to high power, and record the sampled voltages. The online recorded data of this setup is summarized in the following.

The sampled outputs start to change at about 1.5 min after the high power (900 W) is turned on, and the change stops at about 3 min, 20 s. When the rapid change starts, strong oily smelling gases are emitted. At the starting point of the rapid change, the thermocouple indicates a critical temperature T_c of 450°C. During the fast changing period, three sets of data of the sampled outputs and the monitored temperatures are recorded as shown in Table I. With these data at hand, we can then calculate the unknown thermal coefficient $\bar{X}$ of the oil-shale dielectric constant under a fast heating process.

Figs. 9–11 are phasor diagrams constructed according to the three columns of the D data in Table I. S_1 and S_3 are parts of circles (with centers at C_1 and C_3) corresponding to the ratio of $2R/1R \equiv (D_1/D_2)^{1/2}$ and $2R/3R \equiv (D_2/D_3)^{1/2}$. Square root is used here because of the detector square-law characteristics. In practice, these diagrams were constructed over Smith charts such that $\bar{z}_{in}$ (corresponding to point R) and $\bar{y}_{in}$ (diametrical point of R)

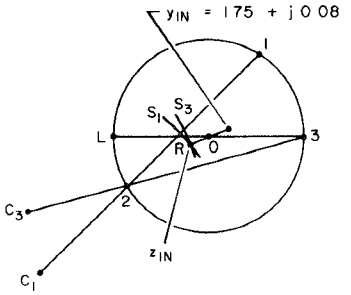

Fig. 9. Phasor diagram with sampled outputs: $D_1=9.0$, $D_2=3.24$, and $D_3=7.9$ (approximately to scale).

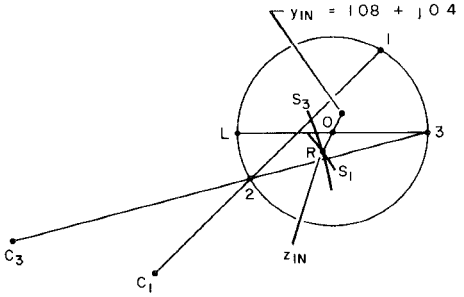

Fig. 10. Phasor diagram with sampled outputs: $D_1=11.8$, $D_2=6.87$, and $D_3=13.9$ (approximately to scale).

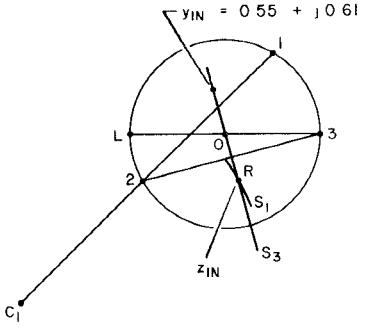

Fig. 11. Phasor diagram with sampled outputs: $D_1=12.1$, $D_2=12.1$, and $D_3=22.8$ (approximately to scale).

could be read off from the charts immediately. As can be shown numerically using asymptotic expansions of Bessel functions, the temperature coefficient $\bar{X}$ of the dielectric constant defined in (5) for our particular oil-shale samples can be determined by the following simplified equation.

$$\bar{X}=0.4\left(\frac{2-\bar{y}_{\text{in}}}{\Delta T}\right) \tag{15}$$

where $\Delta T \equiv T_0 - T_c$ is the temperature increment beyond the critical temperature at the entrance surface of the oil shale. T_c is the temperature we recorded when rapid change started, and $T_c=450°C$. Therefore, ΔT for each column of data in Table I is 19°, 61.5°, and 98°, respectively. With these ΔT's and the $\bar{y}_{\text{in}}$'s calculated in Figs. 10–12, we can calculate $\bar{X}$ easily from (15). The result is that corresponding to each column of data in Table I, $\bar{X}$ is equal to (unit is $(°C)^{-1}$)

$$(5.26-j1.7)\times 10^{-3} \quad (5.99-j2.6)\times 10^{-3}$$
$$(5.9-j2.49)\times 10^{-3}$$

respectively. Thus $\bar{X}$ is approximately constant in the fast heating process. The nominal constancy of this temperature coefficient of the dielectric constant is therefore a quantitative support to the theory proposed in Section I. Other experiments on kerogen chemical analysis during pyrolysis studied by Duvall and Jensen [13] also showed similar rapid temperature-dependent changes as those shown in Fig. 3.

IV. Conclusion

When oil shale is subject to fast microwave heating, the changes of the dielectric constant and other physical properties with respect to temperature and time are abrupt. With a coaxial waveguide system and the qualitative behavior of the fast changing $(\bar{\epsilon}-T)$ variations, we are able to arrive at an online scheme for measuring quantitatively the $(\bar{\epsilon}-T)$ variations. Our preliminary online measurements show an encouraging result that supports a proposed theory explaining this fast changing characteristic from the point of view of competitive chemical kinetics.

Acknowledgment

The author wishes to acknowledge the following institutes and persons: the Laramie Energy Research Center and Dr. I. Jacobson for their periodical review and constructive suggestions, E. Wall and F. Barnes, who helped to fund this particular project as a part of a larger program, and C. Johnk for stimulating discussions.

References

[1] S. Glasstone, *A Text Book of Physical Chemistry*, 2nd Ed. Princeton, NJ: Van Norstrand, 1959, pp. 1098–1104.
[2] N. Davidson, *Statistical Mechanics*. New York: McGraw-Hill, 1962, ch. 7.
[3] W. Gruse and D. Stevens, *Chemical Technology of Petroleum*. New York: McGraw-Hill, 1966, ch. 9, p. 353, p. 361.
[4] R. Hengstebeck, *Petroleum Processing*. New York: McGraw-Hill, 1959, ch. 6, p. 124, p. 126.
[5] P. Ostergaard and E. Suroley, *Refiner Nat. Gasoline Mfr.*, vol. 19, p. 301, Sept. 1940.
[6] Geniesse and Reuter, *Ind. Eng. Chem.*, vol. 22, p. 1274, 1930.
[7] M. Abramowitz and I. Stegun, *Handbook of Mathematical Functions*. New York: Dover, 1965, p. 375, (9.6.10); p. 376, (9.6.26–4); p. 257, (6.1.37).
[8] W. J. Duffin, *Wireless Engineer*, pp. 317–32/, Dec. 1952.
[9] E. L. Ginzton, *Microwave Measurements*. New York, McGraw-Hill, 1957, pp. 303–307.
[10] D. D. King, *Measurements at Centimeter Wavelength*. Princeton, NJ: Van Nostrand, 1952, pp. 197–200.
[11] G. F. Engen, "Determination of microwave phase and amplitude from power measurements," *IEEE Trans. Instrum. Measurements*, IM-25, pp. 414–418, Dec. 1976.
[12] ——, "Calculation of an arbitrary sex-post junction for measurement of active and passive circuit parameters," *IEEE Trans. Instrum. Measurements*, IM-22, pp. 295–299, Dec. 1973.
[13] J. Duvall and H. Jensen, *Colorado School of Mines Q.*, vol. 70, pp. 202–204, July 1975.